Proceedings of ASME Turbo Expo 2011
GT2011
June 6-10, 2011, Vancouver, British Columbia, Canada

GT2011-46219

INVESTIGATION OF THE SURGE BEHAVIOR OF A MULTI-STAGE AXIAL COMPRESSOR WITH A MULTI-SENSOR PROBE

P. Waniczek
P. Jeschke
Institute of Jet Propulsion and Turbomachinery
RWTH Aachen University
D-52062 Aachen, Germany
Email: waniczek@ist.rwth-aachen.de

H. Schoenenborn
T. Metzler
MTU Aero Engines GmbH
D-80995 Munich, Germany
Email: harald.schoenenborn@mtu.de

ABSTRACT

The surge behavior of the first rotor of an eight-stage aero engine high pressure compressor has been investigated experimentally. For that purpose, a new multi-hole pressure probe was developed and adapted to the axial compressor test rig. Due to the high time resolution measurements (more than 45000 measuring points per surge cycle) it is possible to investigate the dynamic flow field of a surge cycle in a time-accurate manner. The results especially show the complex flow field structure at the surge inception. At the rotor leading edge the flow shows perturbations with high amplitudes and initiates the surge event, whereas the flow at the rotor trailing edge is less influenced. The inflow vector turns around the leading edge of the blade relatively slowly. During that turn around three different characteristic flow conditions have been identified. These are ‘zero rotor turning’, ‘turbine-like flow’ and ‘no flow’. ‘No flow’ means, that the absolute velocity vector reaches a flow angle where it consists of a pure tangential velocity component. That is the point where the reverse flow phase is initiated. A 180° shift of the flow direction at the rotor trailing edge is the consequence. After a quasi-steady reverse flow the acceleration of the flow starts.

In total, this paper gives new and fundamental insights into the unsteady flow field phenomena during various surge cycles. Especially the transient velocity vector imparts a good idea of the flow field structure of a surging compressor.

INTRODUCTION

Two different types of compressor instabilities exist mainly, stall and surge. Stall is a phenomenon that is local to the compression system. In contrast to stall, surge affects the whole compression system and can lead to fatal damage of blades and/or the whole compressor. A lot of work has been done on stall effects, because that phenomenon is easier to investigate experimentally and the risk of damaging the compressor is lower compared to surge. In the past years compressors are built to resist loads induced by surge and therefore experiments could be performed under surge. At the same time, computational methods and capacities have reached a level to resolve the complex flow fields of stall and surge events. Nevertheless, there exists a lack of experimental data to validate CFD-results of surge cycles. A lot of investigations have been conducted on the behavior of the whole compression system under surge. One of the first was Greitzer [1] who characterized compression systems and their instability behavior as a whole. With an increase of computational methods and capacities nowadays, it is possible to calculate stall and surge transients of compression systems [2]. Vahdati et al. [3] for example were able to investigate the compressor numerically in rotating stall and surge conditions. Their numerical and experimental results matched well. Less information is given in the open literature about the dynamic flow field during the surge event in the blade passages of compressors. This flow field is characterized by high unsteadiness and amplitudes especially at the onset of surge and the recovery process. Gamache and Greitzer [4] performed measurements in a reversed through flow three-stage compressor. They were able to show stage characteristics and velocity vectors for steady reversed flow. Day [5] and Greitzer [6] used hot wires to measure velocity components in axial compressors during surge cycles at different axial positions. Most other experimental work uses instrumentation in the casing and therefore cannot gain information of the flow field during surge.

This study will present a new multi-hole probe that was developed to resolve the unsteady flow field during the surge cycle. Due to the installation space needed, the probe was located in the axial gaps before and after the first rotor of an eight-stage high pressure aero engine compressor. In combination with a special calibration procedure this new probe is capable to resolve a transient 360° flow field, characterized by flow angle, Mach number, total and static pressure. The results give a high time-resolved overview of the dynamic flow field phenomena of a rotor in all phases of the surge cycle, including deceleration, negative flow, acceleration and normal flow [5].

NOMENCLATURE

A	probe downstream of the rotor
B	probe upstream of the rotor
BPF	Blade Passing Frequency
CFD	Computational Fluid Dynamics
FFT	Fast Fourier Transform
IGV	Inlet Guide Vane
Ma	Mach number
R	rotor
RS	rotating stall frequency
S	stator
U	voltage
VGV	Variable Guide Vane
f	frequency
p	pressure
r	residuum
rev	revolution
u	rotor speed
α	tangential flow angle of fluid flow
abs	absolute
meas	measured
probe	values of probe
ref	reference
stat	static
t	total
trav	traverse unit
x	axial

MULTI-SENSOR PROBE

Design

For the investigation of the unsteady flow field of a surging compressor the Institute of Jet Propulsion and Turbomachinery at RWTH Aachen University designed and manufactured two identical multi-sensor probes. The boundary conditions for such probes are predetermined by the flow field and listed in the following:

1) Reversed flow, which results in a 360° resolution of the flow field
2) High unsteady flow field within a wide range of velocities
3) High temperature rise during the surge cycle of hundreds of Kelvin's
4) High mechanical load on the probe shaft and measurement technique
5) Forcing of vibrations

The first boundary condition results in a symmetric probe cross section, which would be similar to a cylindrical probe. Therefore, the probe head is designed as a nonagon with a length of 40 mm. The cross section of the measurement head of the probe is shown in Figure 1.

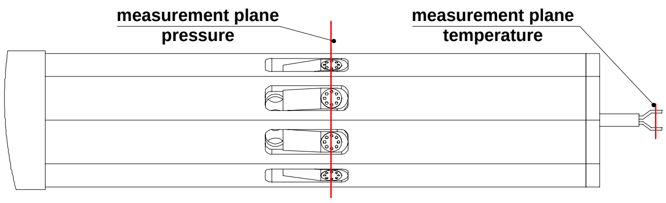

Figure 1: Cross sectional view of the probe head

The head consists of two different measurement planes. The upper measurement plane is used for measuring the unsteady pressure distribution around the annulus of the probe. With a calibration polynomial the flow quantities are calculated from these pressure values. For the pressure measurements each of the nine surfaces of the nonagon is equipped with a miniature semiconductor pressure transducer. These pressure transducers are fixed in a groove, so that the sensors´ surface is flush with the surfaces of the nonagon. Since the sensor is right in the middle of the surfaces of the nonagon, the pressure measurement plane is 20 mm above the end of the probe. This is necessary due to the outer diameter of the probe. Hence, the guideline for cylindrical probes is fulfilled, which recommends a specific ratio between outer diameter and distance between the measurement plane and the end of the probe shaft. The nine sensors allow a full 360° resolution of the flow field. The advantage of the shown design is that the sensors are directly located in the flow field. This results in a low signal to noise ratio and a minimum of signal damping caused by dead volumes. The resolution of the sensors is ±100 Pa with a maximum pressure range of $7{*}10^5$ Pa (100 psi). The compensated temperature range is between -55 °C and 235 °C. The second measurement plane is used for measuring the transient temperature rise along the surge cycle. For that purpose, the tip of the probe is equipped with a transient temperature sensor. This sensor is located in the center line of the probe and manufactured as a miniaturized thermocouple.

Due to the forced mechanical loads and vibrations the shaft of the probe has to be robust. Therefore, ahead of the measurement plane it is designed as a circular tube.

Calibration procedure and data acquisition

The calibration of the pressure transducers and thus the calibration of the probe are carried out in two steps. First, the pressure transducers are calibrated in a static manner. For that purpose, the head of the probe is installed in a pressure-tight vessel. Beginning at ambient pressure, the pressure in the vessel is increased in $1*10^4$ Pa increments until $5*10^5$ Pa absolute. This pressure range is sufficient, because in the compressor a maximal total pressure of $3*10^5$ Pa is estimated at the measurement location. The pressure in the vessel is measured by a PSI-module with an accuracy of $4*10^2$ Pa. At each pressure level the measurement voltages of all nine transducers are recorded by a digital multimeter. The measurement accuracy of the multimeter used is $9*10^{-4}$ V and therefore higher than the accuracy of the pressure transducers. The relationship between pressure levels and measurement voltage is shown in Figure 2. All transducers have a linear characteristic which can be approximated by a linear equation. For each sensor an individual approximation is made. The maximal residuum of all linear equations is less than r=0.99999.

After the static calibration of the transducers a dynamic calibration of the probes is carried out. From this calibration polynomials are gained for the flow angle, Mach number, total pressure and static pressure. For that purpose, the probe is installed in a traverse unit right in the middle of a free jet. With the traverse unit the probe is rotated 360° around its center line in 2° increments. Thus, 180 data sets are generated for characterization of the probe. The rotation around the center line is carried out at seven Mach numbers in-between a wide subsonic range in 0.1-Mach increments. The chosen Mach-interval is in the recommended range for cylindrical probes. This Mach-interval also corresponds with the high subsonic Mach numbers, which are present in modern high pressure compressor front stages. Nevertheless, the flow field during the surge cycle is characterized by a wide range of Mach numbers, beginning at zero up to transonic conditions. For these extreme flow conditions the calibration polynomial has to be extrapolated.

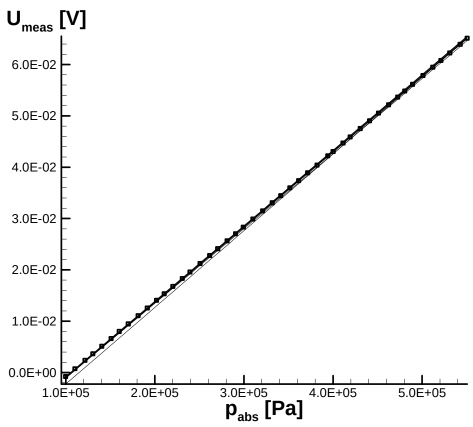

Figure 2: Static calibration of pressure transducers

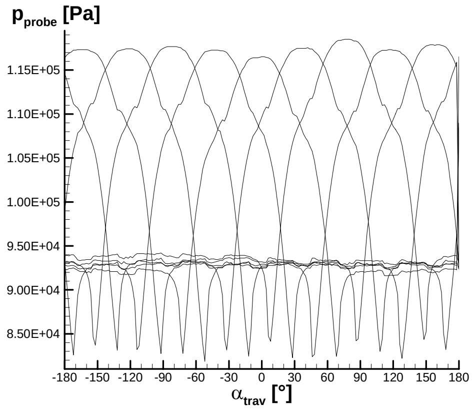

Figure 3: Free jet calibration of the multi-sensor probe

The result of the dynamic calibration for one specific Mach number is shown in Figure 3. The measurement voltages are transformed into pressure values by the linear equations of the static calibration. The mean absolute deviation of the nine pressure peaks is ±150 Pa. Therefore, it is necessary to calculate a specific polynomial for each sensor triple. The probe is divided into nine sectors with a range of ±20° and the sensor position in the middle. For all of the nine segments calibration polynomials are calculated for the area of 20° left and right of the peak. In total, this procedure builds nine virtual three-hole-probes around the circumference of the probe with a calibration range of ±20°. Nevertheless, it must be identified which virtual three-hole probe is representative for the fluid flow. For that purpose, it is assumed that the main flow direction is indicated by the maximal measured pressure around the probes´ circumference. The curves of Figure 3 show that this assumption is valid. Therefore, the sensor which measures highest pressure is chosen as the middle sensor of the virtual three-hole probe. For calculation of the polynomials and flow quantities the sensors to the right and left of that position are taken into consideration and evaluated. The nomenclature of the virtual three-hole-probes is listed in Tab. 1. As shown in

Tab. 1: Evaluation of calibration and measurement data

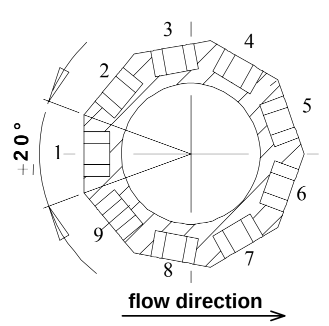

central sensor	left sensor	right sensor
1	9	2
2	1	3
3	2	4
4	3	5
5	4	6
6	5	7
7	6	8
8	7	9
9	8	1

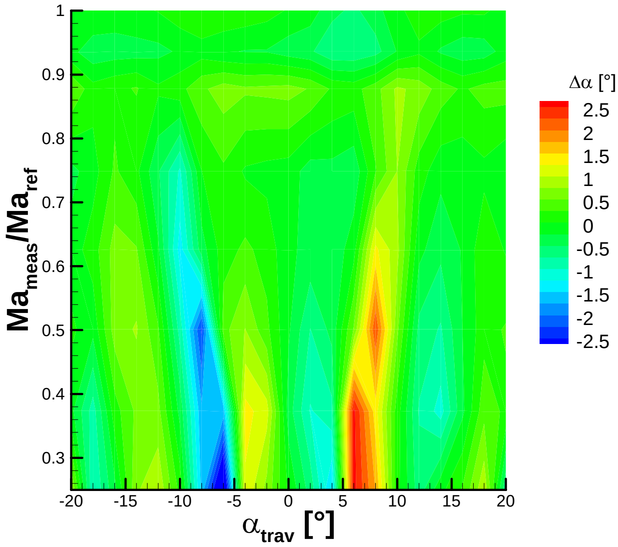

Figure 4: Error in calibration polynomial (flow angle)

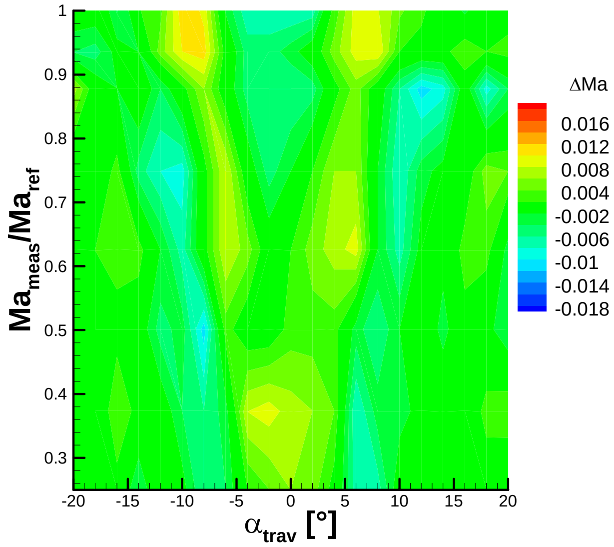

Figure 5: Error in calibration polynomial (Mach number)

Figure 3 the course of pressure of the middle sensor is relatively flat, which would mean insensitivity to the angle of attack. This disadvantage is compensated by the outer sensors. These two sensors have a high gradient in that region and make a definite correlation between the pressure-triples and flow quantities (calibration polynomial and evaluation procedure) possible.

The spatial resolution of the measurements performed is defined by two means. First, the measuring area is defined by the surface spanned by the height of the pressure transducers and distance between the two outer sensor positions of the virtual three-hole-probe. This area has an extension of 9.6 mm^2 and is characterized by a flat square. Second, the spatial resolution is defined by the dimensions of the pressure transducer. The chosen type has a screen for protection. The pressure value is therefore an averaged value over an area of 2 mm^2.

In total, nine calibration polynomials are generated. The quality of these polynomials is characterized by the error bars. For one virtual three-hole probe the errors of the flow angle and Mach number are given in Figure 4 and Figure 5. The abscissa shows the angle of rotation given by the traverse unit in the free jet. The ordinate represents the seven normalized Mach numbers at which the probes are calibrated. The contour displays the absolute error of the calibration polynomial for the field spanned by Mach number and angle. In the region of +8° and -8° the error in flow angle is the highest. These errors are caused by the sharp edges of the nonagon. This is pronounced at low Mach numbers. For higher Mach numbers the errors decrease rapidly. In all other regions of the field the absolute errors are less than 0.8°. The polynomial for the Mach number shows similar effects of the sharp edges, but the errors caused are less than Ma=0.01. For high Mach numbers the highest errors are identified. In total, the polynomials have a good quality. The root-mean-square deviations of flow angle, Mach number, total pressure and static pressure are listed in Tab. 2. The deviations in the polynomials for the four flow quantities are in the range of common pneumatic probes. An exception is the polynomial for the static pressure, whose deviation is a little bit higher compared to conventional multi-hole probes. The authors want to clearly say, that the discussed accuracies are only related to the approximation of the calibration polynomials and do not represent the overall accuracy of the whole measurement chain, e.g. influence of unsteady phenomena.

Tab. 2: Sum of root-mean-square error of calibration polynomials

	α	Ma	p_t	p
Sum of root mean square error	0.495°	0.004	63 Pa	265 Pa

For both calibration procedures, the static and dynamic one, the measurement voltages of the pressure transducers are logged by a digital multimeter, which means a steady state situation. Since the surge event has a high unsteady character, the measurement voltages during the measurements at the compressor test rig are recorded transiently. The signals of the pressure transducers are sampled with 102.4 kHz. Due to the lower time resolution of the transient temperature sensor, the signal of the temperature sensor is recorded with 6.4 kHz.

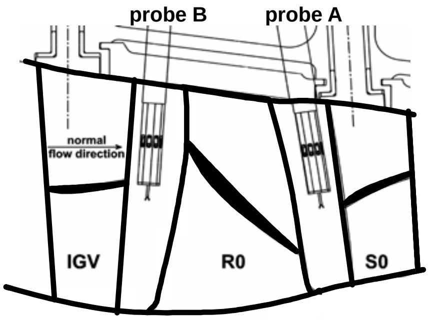

Figure 6: Sketch of the front stage of the rig with mounted probes

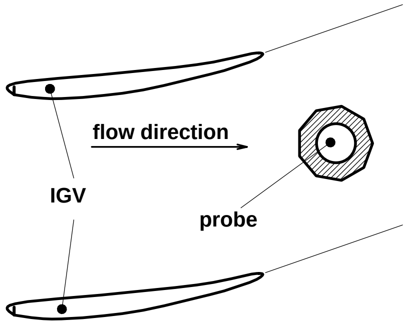

Figure 7: Proportion between probe and blade passage

TEST FACILITY

Compressor Test Rig

After calibration the multi-sensor probes are adapted to an eight-stage axial compressor. This research compressor is designed regarding a high pressure aero engine compressor. The first three stators, including the inlet guide vane (IGV), are variable vane rows. The compressor ingests air from the ambient. After a plenum chamber, which can be evacuated for regulating the inlet pressure of the compressor, the flow enters the engine. When surge is detected, a protection valve opens to discharge the compressor.

Two identical multi-sensor probes are mounted to the compressor simultaneously. Due to their size they can only be installed in the front part of the compressor. The axial spacing and channel height in this region is larger than in the rear part of the machine. One probe is mounted upstream, the other one downstream of the first rotor. In circumferential direction the probes have a distance of 20°. This is necessary, because the probes should not have an impact on each other. Due to their distance of 20° each probe is located in a separate blade passage. Figure 6 shows a cross sectional view of the compressor with mounted probes in front of and behind the first rotor. The probe accesses are inclined following the angle of the leading and trailing edge of the blade. For the measurements performed the probes are positioned at two different channel heights. Regarding the measurement plane of the pressure sensors they are positioned at 50% and 70% span, respectively. Since the temperature measurement plane is not congruent with the pressure measurement plane, the temperature sensor is on a lower channel height. Tab. 3 summarizes the radial positions of both measurement planes. For the 50% configuration (referring to pressure sensor plane) the temperature sensor is on 25% to 30% channel height, for the 70% configuration in the mid-span region.

Tab. 3: Radial position of pressure and temperature sensor (% channel height)

	ahead of rotor		behind rotor	
pressure sensor	50%	70%	50%	70%
temperature sensor	29%	49%	24%	44%

In total, data are gathered during several different surge events, regarding the rotational speed and VGV schedule. The compressor is throttled at several different speed lines between 75% and 100% design speed until surge occurs. Specific speed lines are chosen, because the relatively huge probes, compared to a blade passage, are very sensitive to wakes. This is especially true for the first probe which is located downstream of the IGV. The selected speed lines offer an IGV schedule that the probe is not affected by the IGV wake.

Figure 7 shows the real proportion between probe and blade passage for the position of the anterior probe at mid-span. The probe covers less than a quarter of the blade passage. With increasing radial position of the probe the ratio further increases. For most of the measurements performed, data are taken from both channel heights. During the whole test campaign both probes are mounted simultaneously.

Impact of probe on compressor performance

The multi-sensor probe is larger than conventional pneumatic probes, e.g. five-hole probes. Therefore, the influence of the two multi-sensor probes on the overall compressor performance is analyzed. For that purpose, additional measurements are performed, which are:

1) mass flow rate measurement of compressor
2) temperature measurements in the compressor exit

The above listed measurement series is performed with different probe configurations. First, the compressor is stabilized at a steady operating point at high speed. Then the probe in front of the rotor is radially traversed until the pressure measurement plane is located at 50% channel height. During that procedure no influence on pressure ratio and mass flow rate could be identified. The same procedure is carried out with the second probe which is located behind the rotor (with the previous probe still inserted). At that time the mass flow rate decreases by 2%. Similar observations show the total temperature distribution at the compressor exit. The exit is equipped with total temperature rakes. When the probe behind the rotor is traversed radially into the flow path, one specific temperature measurement location shows an increase of 4%. That indicates that the influence of the probe affects the whole compressor and is even measurable at the compressor exit.

In total, this analysis shows that the probe which is located downstream of the first rotor has an influence on the compressor operating point but for measurements of the reverse flow of a surge event this influence should not dominate the results.

EXPERIMENTAL RESULTS

Before a detailed investigation of the flow quantities is given the raw pressure data will be analyzed first. Figure 8 shows the time traces of the raw data of both probes for 93% speed and 70% channel height. For a better understanding the pressure values are averaged over 50 samples by a moving average method. This method is carried out by averaging the first 50 samples, then samples 2 to 51 and so on. The left graphs belong to the probe that is installed in front of the rotor, the right ones to the probe behind the rotor. On the abscissa rotor revolutions are depicted with the datum point at the beginning of the surge event. This datum point is characterized by the peak pressure of an unsteady wall pressure sensor which is used for reference in all data sets. The relative position between the sensor numbers of the probes and normal flow direction can be seen in Tab. 1 or Figure 12. The rotational direction in the figure is from down to top. Analyzing the region before the surge event by comparing the two upper graphs of Figure 8 (rev<0), the expected pressure rise of the rotor is obvious. Both probes

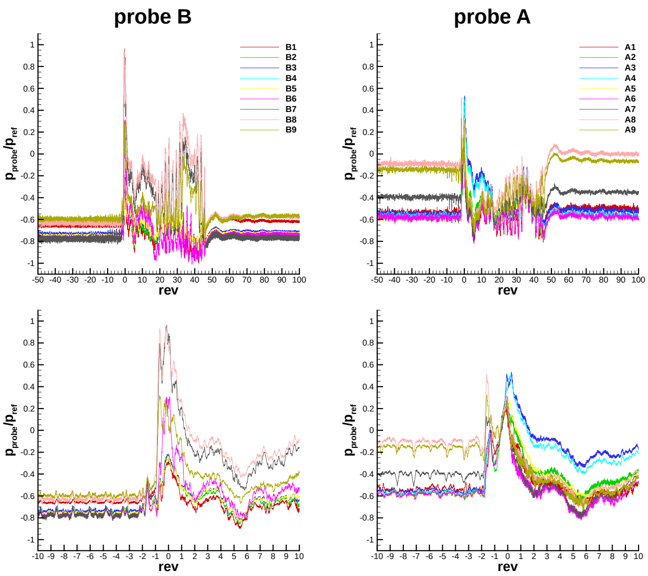

Figure 8: Moving time averaged raw pressure data

show a flow direction that is in the area of sensor #9. Therefore, for that time period the virtual three-hole probe with the sensor numbers 8, 9 and 1 is evaluated. After surge (rev>50) all pressure sensors show similar pressure levels as before surge. The surge cycle has a time period of 50 rotor revolutions, which is common for high pressure aero engine compressors. In the lower graphs of Figure 8 the area of the surge inception is shown in detail. It is obvious that the pressure rise in both pictures is totally different. First, all sensors of probe A indicate an enormous pressure rise two rotor revolutions before the datum point. The second peak at the datum point is present in both graphs, with higher amplitude in the measurement plane in front of the rotor. In contrast to the pressure rise of probe A, probe B shows a minimal change in the flow direction. That is indicated by the highest pressure of sensor #7 during the whole reverse flow phase and even during the whole surge cycle. The second peak in the time trace of probe A is characterized by the highest pressures of sensors #3 and #4. Assuming that the highest pressure around the circumference shows the main flow direction the change of maximal pressure from sensor #7 to sensors #3/4 is equivalent to a 180° turning of the flow field. This direction is forced by the reversed flow-through of the stator. The area between the two peaks is very interesting. It will later be shown, that during the rising slope at rev=0 a total breakdown of the flow occurs behind the rotor. This is indicated by an absolute velocity of zero. This phenomenon is visible in the raw data trace, because at the sliding slope all nine sensors have the same pressure value and no flow direction is dominant. This is also a confirmation of the quality of the extrapolation of the calibration polynomials because raw data and evaluated Mach number yield to the same physical logic. The extrapolation is necessary, because a calibration at Ma=0 is not feasible. After the peak pressure, the pressure of all sensors decreases until the same pressure level is reached at both axial measurement locations. Subsequently, the re-pressurization starts.

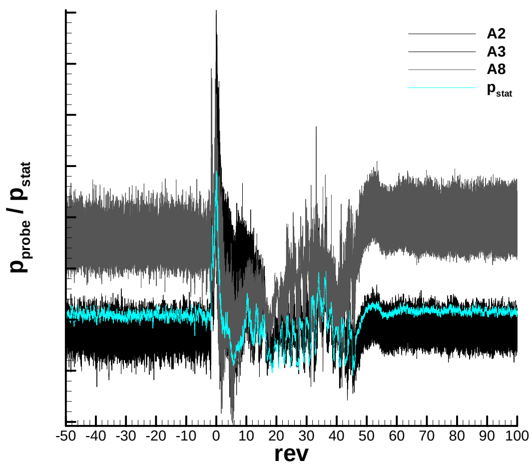

Figure 9: Evaluation of static pressure

A second evidence of the validity of the free-jet calibration is given by the static pressure results. In a previous section it was shown that the polynomial for that flow quantity has the highest mean error. As suggested by Heneka [7] it can be assumed that the sensors in the dead water area measure approximately the static pressure. Heneka developed a probe that is capable to resolve a 3-dimensional unsteady flow field. For balancing of the unsteady pressure sensors used, the probe was turned 180° in the free jet and it could be demonstrated that the sensors show the ambient pressure. This procedure can be devolved to the multi-sensor probe A, for the case of normal flow and also accomplished reversed flow. For the first case a dead water is identified at the sensors #2 and #3, for the second one 180° shifted (sensor #8). In Figure 9 the pressure values of sensors #2, #3 and #8 are displayed together with the calculated static pressure. The static pressure corresponds with the pressure level of the sensors #2 and #3 for the time before and after the surge event. For the case of reversed flow (rev 0–20), the static pressure is calculated with the polynomial of the virtual three-hole-probe (3, 4, 5) and compared to the pressure value of sensor #8. Both values are in good agreement.

As shown above the analysis of the raw data gives a first plausible idea of the flow field during surge. Furthermore, the calibration procedure could be verified and confirmed.

Analysis of frequency spectra

The equipment of the probe head with semi conductive pressure transducers allows a transient recording of pressure data. For the measurements carried out at this specific test rig the sensors are sampled with 102.4 kHz. At design speed this corresponds with twelve measurement points in each blade passage of the first rotor. Hence, the blade passing frequency is resolved. With regard to the Nyquist-criterion the maximal resolvable frequency is 51 kHz which is further reduced by the cut-off frequency of the low-pass filter. This results in a maximal resolvable frequency of 40.8 kHz. For a better understanding of the frequency spectra Figure 10 and Figure 11 show the sliding frequency analysis of sensor #8 of probe B and probe A. The sliding FFT is Flat-Top windowed. The length of each evaluated time window is 0.08 sec (8192 samples) which leads to an accuracy of the frequency spectrum of 12.5 Hz. The time windows are overlapped by 80%.

The blade passing frequency of f/f_{ref}=0.72 of rotor 1 is clearly visible in both frequency spectra (Figure 10 and Figure 11). Just at the beginning of the surge cycle (rev=0) the first blade passing frequency (1. BPF) dominates the spectra up- and downstream of the rotor. Furthermore, low frequencies are excited just prior to surge. Such a shift of dominant frequencies is reported by Longley [8] for a stalled stage. Someone could think that the instability is caused by the probes, but for higher speeds this phenomenon could not be identified. So the authors think that this phenomenon is not caused by the probes and is a property of this special compressor. The onset of the reversed flow leads to an abrupt drop of the amplitude of the 1. BPF upstream of the rotor. Downstream of the rotor the reverse flow phase leads to a decay of the amplitude until nearly zero. At the end of the reverse flow phase the acceleration of the fluid flow starts and a/some rotating stall cell(s) develops, which dominates the frequency spectrum of probe B between rev=17 and rev=46 (RS). The frequency is half the rotor speed. Similar

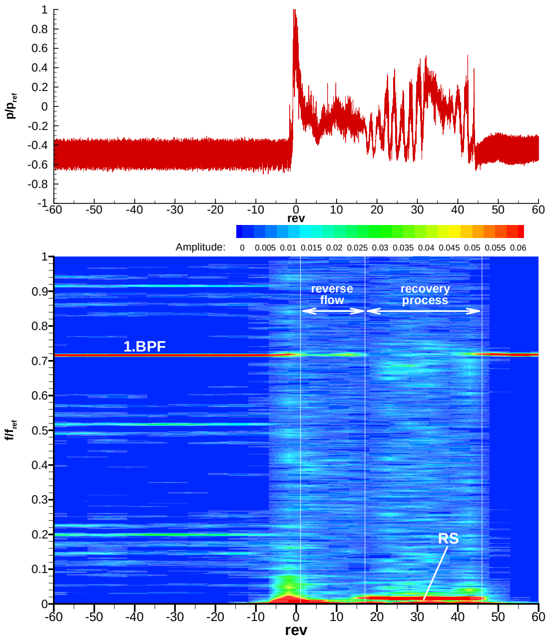

Figure 10: frequency spectrum and corresponding signal of sensor #8 (upstream rotor)

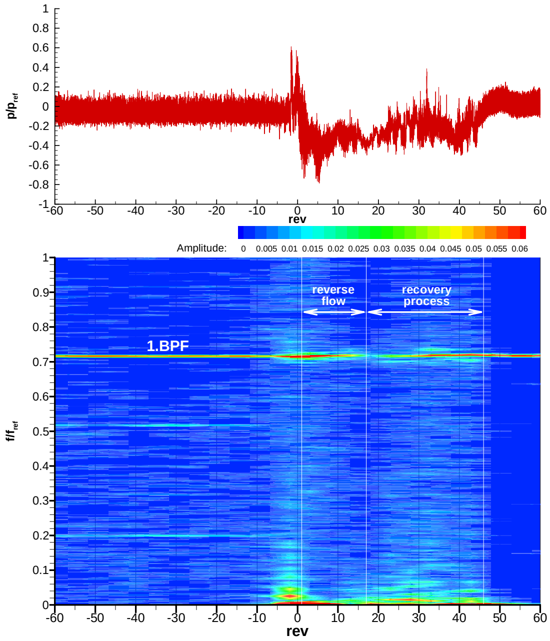

Figure 11: frequency spectrum and corresponding signal of sensor #8 (downstream rotor)

observations are reported by Schlamann [9], who showed a developing of rotating stall during the recovery process in a multi-stage axial compressor. At rev=46 the rotating stall cell disappears and the flow field is stable. At that time the frequency spectra are dominated by the 1. BPF.

To be sure that the discussed frequencies are not caused by the introduced probes, unsteady wall pressure at different circumferential and axial positions around the first rotor is measured twice (with and without mounted multi-sensor probes). A comparison of the frequency spectra of these two measurements shows the same characteristic frequencies as Figure 10 and Figure 11. Therefore, an influence of the probes on the detected frequencies can be excluded.

Surge cycle of the compressor

In this chapter a detailed analysis of the surge cycle will be given. For that purpose, the moving averaged pressure data of Figure 8 are transformed into flow quantities by the calibration polynomials that are shown in one of the previous chapters. For a better understanding of the results Figure 12 shows a sketch of the blading with mounted probes and the convention of the flow angle and flow direction. Angles between 90° and 270° indicate a back flow, the other 180° normal flow.

Figure 13 shows the time trace of the absolute flow angle for one surge cycle. The lower graph displays the complete surge cycle, whereas the upper graph shows in detail the first eight rotor revolutions of the surge event. The orange course belongs to the probe upstream of the rotor, the green one to the probe downstream of the rotor. It is obvious that the flow field in front of the rotor is characterized by higher fluctuations. These fluctuations are typical before stall and surge [10], [11]. The amplitude of these perturbations rises until the whole compression system is unstable and surge occurs [12]. The development of reversed flow is clearly shown by the green graph (behind the rotor). In-between approximately two rotor revolutions the flow turns from normal to reversed conditions (time steps 2–7). It is conspicuous that the flow angle in front of the rotor changes relatively slowly and continuously when surge is initiated. Behind the rotor the flow angle rises on a level that is nearly 20° higher than that at normal flow conditions. At the time when the flow at the rotor inlet consists of a pure tangential velocity component (α=240°) an abrupt turning of the flow direction at the rotor exit of approximately 240° occurs. After that phase a long period of reversed flow is

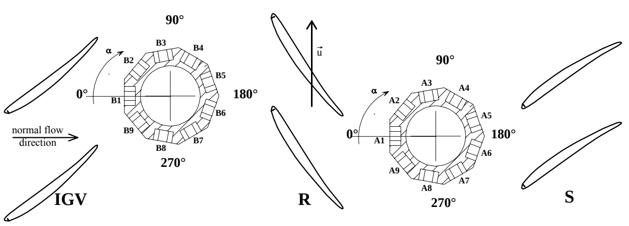

Figure 12: Sketch of blading, probe positions and convention of flow angle

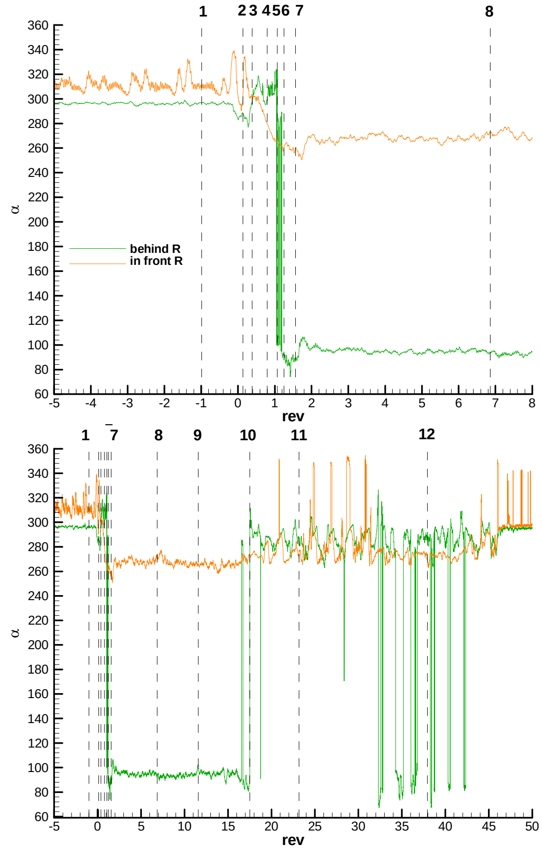

Figure 13: Absolute flow angle during surge cycle

observable indicated by the relatively constant flow angle. At time step 10 the flow turns back into normal flow direction. This time the turning is very abrupt. Similar observations are reported by Day [5]. After this second turning the flow is not stable.

It seems that the re-pressurization of the plenum volume is not completed. First, an unstable flow field is established in front of the rotor and a stable one behind the rotor (time step 11). Then the flow field is characterized vice versa (12). Both periods have a duration that is similar to the reverse flow phase of approximately 15 rotor revolutions. This phenomenon is identified as a rotating stall cell also shown in the frequency spectrum of Figure 10.

For a more detailed analysis of the flow field during surge Figure 14 shows twelve discrete time steps of the surge cycle. The numbering of time steps in Figure 14 corresponds to that in Figure 13. Displayed are two velocity vectors, one for the flow in front of the rotor and one for the flow behind the rotor. The vectors are drawn in a polar coordinate system by the measured flow angle and absolute Mach number. The direction of the vectors is always from the outside to the center. Each number of the angle-scale corresponds with one of the nine sensors. The datum point represents a flow that is parallel to the center line of the compressor (normal flow direction).

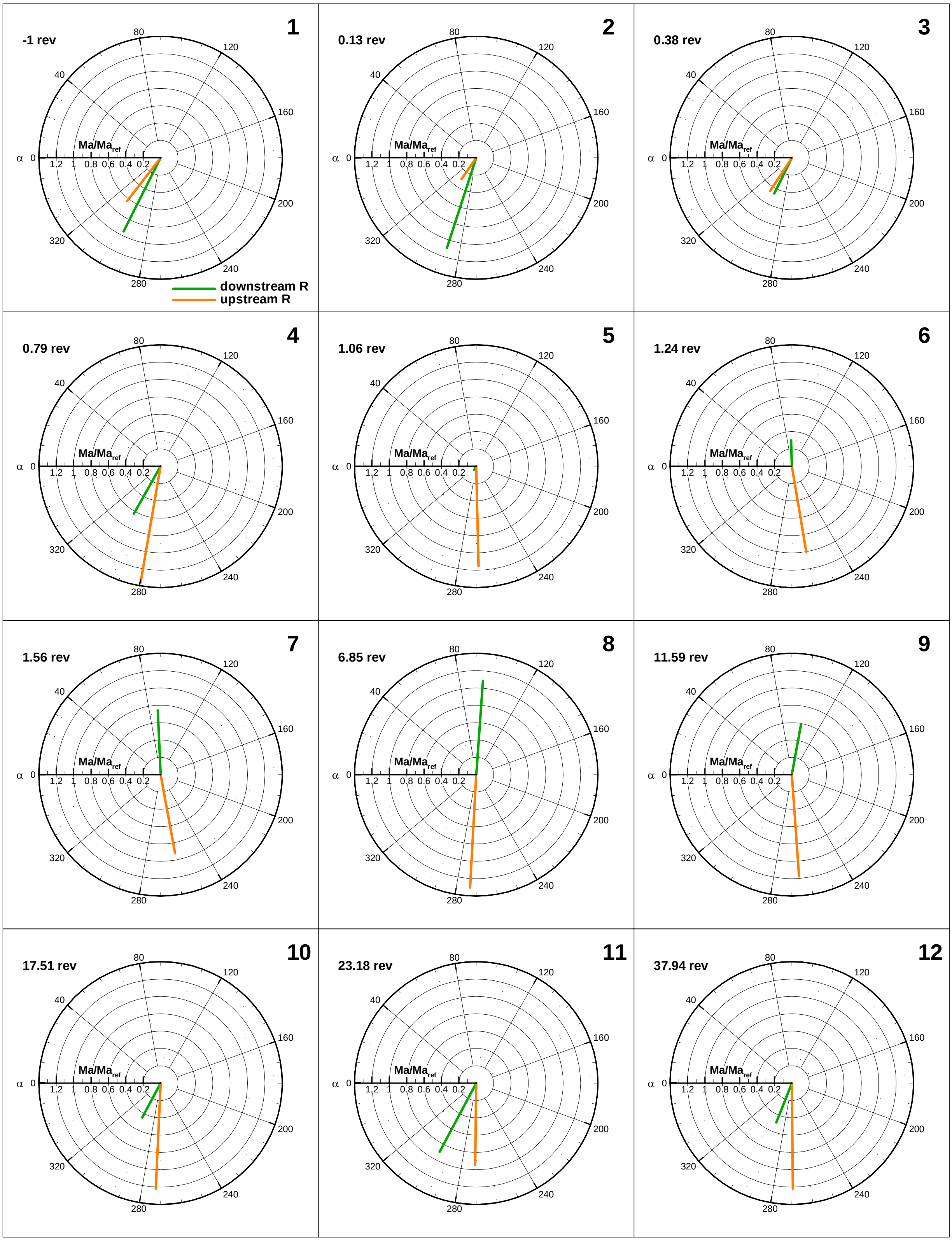

Figure 14: Velocity vectors in front of and behind the first rotor during a surge event

In the following paragraph the twelve time steps of Figure 13 and Figure 14 will be analyzed in detail.

Time step 1: normal flow
Just one rotor revolution before surge inception the rotor is still absorbing work and transferring energy to the air. This is indicated by the positive flow angle when assuming that the tangential velocity component u is equal in front of and behind the rotor.

Time step 2: surge initiation
At the rotor inlet the perturbations reach the maximum amplitude which leads to high incidence angles and to a separated flow. Therefore, surge is initiated. The flow field at the rotor exit is not affected extensively by that phenomenon. Due to a reduced mass flow rate and the separation the absolute flow direction changes minimally to higher incidences.

Time step 3: zero rotor turning phase
After more or less half a rotor revolution the transferring of energy to the fluid flow is zero. The absolute velocity components at the rotor inlet and exit are absolutely the same. Assuming that the tangential velocity component u at the inlet and exit is equal, this consideration leads to congruent velocity triangles.

Time step 4: turbine-like flow
At this time step the angle of the absolute velocity vector at the leading edge turns backward and crosses the velocity vector of the trailing edge (orange vector lies on the right side of the green one). This leads to a high incidence and the incoming flow impinges the suction side of the rotor blade which results in flow conditions similar to turbine blades. That means that the tangential velocity component in the stator frame at the leading edge is higher than at the trailing edge. Since the rotation of the rotor represents an extreme resistance for the fluid flow, a breakdown of the flow regime occurs rapidly.

Time step 5: no flow
Approximately one rotor revolution after the surge process is initiated a total breakdown of the flow field is observable showing a zero-crossing of the axial velocity. The axial velocity component is zero for both vectors, behind the rotor that is even the case for the absolute velocity. This results in a stagnation of the fluid flow for a short time period. In contrast to an absolute stagnation of the flow behind the rotor, the flow in front of the rotor is characterized by a pure tangential velocity component.

Time steps 6/7: reverse flow inception
Between these two time steps a reversed through flow of the rotor develops. This phase is characterized by a separated flow of the upstream stator, indicated by absolute flow angles of less than 90°. The rotor still impresses a tangential velocity component to the fluid flow by further rotation. This has a direct impact on the flow field at the rotor inlet. The rotor transfers energy to the system during the reversed flow. Therefore, the relative and tangential velocity components are added and this results in an extreme high absolute velocity vector. These observations are in accordance with those from di Mare et al. [13].

Time steps 8/9: fully developed reversed flow
Between time steps 7 and 10 the reverse flow is clearly visible. The rare fluctuation of the flow angle shows the quasi-steady characteristic of the developed reversed flow. In accordance to Gamache and Greitzer [4] the flow is guided by the stator, which is confirmed by these results. During the reverse flow phase an acceleration and deceleration of the fluid flow occurs. That is indicated by the waxing and waning of the Mach number with a maximum at time step 8 (see time steps 7–9)

Time step 10: Acceleration
The reverse flow phase ends very abruptly which is a known phenomenon [5]. The zero-crossing of the axial velocity component is hard to see. The shift of the flow angle at the trailing edge is nearly 180°, similar to the onset of the backflow. Here, the flow stabilizes quickly whereas the flow field at the rotor inlet is still dominated by a tangential velocity component.

Time steps 11/12: post surge
After the acceleration of the fluid flow and development of a normal flow direction the compression system is still in an unstable status (time step 11). At revolution 32 a more or less homogenous incident flow at the rotor inlet is developed. The flow field at the trailing edge is furthermore characterized by high unsteadiness. It seems that the rotor stalls probably caused by the moving stators and the reaction of the protecting valve. This assumption is in addition with the transient temperature measurements. After a pronounced temperature peak caused by the surge event a second flat peak is detected. This peak is temporally in accordance with the unstable interval after the surge event.

CONCLUSION

From the research described and discussed in this paper the following conclusions may be made:

- The multi-sensor probe, that was specially designed for this research project, is capable to resolve the unsteady flow field 360° and is therefore usable to investigate the surge cycle of a compressor in a time-accurate manner.
- The calibration and evaluation procedure applied could be verified by comparing the calculated static pressure with the pressure in the dead water area of the probe. Furthermore, the extrapolation of the polynomials, which is necessary due to a zero-cross of the velocity vector, was quantified. It could be demonstrated that zero velocity was

detected when all nine sensors of the probe indicated the same pressure value.

- The raw pressure data give a first idea of the flow field during surge in front of and behind the rotor. The observations drawn from these raw data were confirmed by the later derived flow quantities.
- The results show that the flow field at the leading and trailing edge of a compressor blade during surge is totally different, especially at the onset of surge. The flow field at the rotor inlet is characterized by high velocities and a relative minor turning of the absolute flow angle of 'only' 50°. When the flow angle reaches 270°, which means a pure tangential velocity vector, a total breakdown of the fluid flow occurs. This leads to an abrupt change of the flow direction at the rotor exit of approximately 240° and the development of the reverse flow phase.
- Three characteristic time steps between the surge inception and reversed flow could be identified. These are 'zero turning phase', 'turbine-like flow' and 'no flow'. Once the flow field is unstable and separated, there exists a condition where the rotor does not transfer energy to the system, resulting in congruent velocity triangles at the leading and trailing edge of the rotor. As a consequence, flow conditions similar to turbines are reached, which is not possible due to the rotational direction of the rotor. This initiates a breakdown of the fluid flow and the reverse flow phase indicated by the zero-crossing of the axial velocity component ('no flow').
- Because of a constant flow angle during the established reverse flow phase, the flow during this phase can be described as quasi-steady. The flow out of the stator into the rotor is guided by the stator itself. At the rotor inlet the relative and tangential velocity component are added which results in a high and steep absolute velocity vector. Similar observations were made by di Mare et al. [13]. The reverse flow ends with a quick acceleration of the fluid flow, which is a known phenomenon [5].
- Nevertheless, a disadvantage of the presented probes is the fact that they can only measure in a 2-dimensional way instead of 3-dimensional. That would be especially important for the beginning and the end of the reverse flow where the flow field is highly 3-dimensional. Furthermore, the discussed results are only related to one specific channel height.

ACKNOWLEDGMENTS

The work published in this paper was partly funded by the German government within the frame of the research program Lufo 4. This is gratefully appreciated.

REFERENCES

[1] Greitzer, E. M., 1976. "Surge and Rotating Stall in Axial Flow Compressors – Part 1: Theoretical Compression System Model". *Journal of Engineering for Power*, **Vol. 98**, pp. 190-198

[2] Longley, John P., 2007. "Calculating Stall and Surge Transients", ASME paper GT2007-27378. Proceedings of ASME Turbo Expo May 14-17, 2007, Montreal, Canada

[3] Vahdati, M., Simpson, G., Imregun, M., 2008. "Unsteady Flow and Aeroelasticity Behavior of Aeroengine Core Compressors During Rotation Stall and Surge". *Journal of Turbomachinery*, **130**, pp. 1-9

[4] Gamache, R. N., Greitzer, E. M., 1990. "Reverse Flow in Multistage Axial Compressors". *Journal of Propulsion*, **6**, pp. 461-473

[5] Day, I. J., 1994. "Axial Compressor Performance During Surge". *Journal of Propulsion and Power*, **10**, pp. 329-336

[6] Greitzer, E.M., 1976. "Surge and Rotating Stall in Axial Compressors – Part II: Experimental Results and Comparison with Theory". *Journal of Engineering for Power*, **98**, pp. 199-217

[7] Heneka, A., 1983. "Entwicklung und Erprobung einer Keilsonde für instationäre dreidimensionale Strömungsmessung in Turbomaschinen". These doktor-ingenieurs, Universität Stuttgart, Germany

[8] Longley. J.P., Hynes, T. P., 1990. "Stability of Flow Through Multistage Axial Compressors". *Journal of Turbomachinery*, **112**, pp. 126-132

[9] Schlamann, U., 1985. "Experimentelle Untersuchung der Strömungsphänomene des Rotating Stall und des Pumpens bei mehrstufigen, hochbelasteten Axialverdichtern". These doktor-ingenieurs Fortschritt-Bericht VDI Reihe 7: Nr. 91, VDI-Verlag, Düsseldorf, Germany

[10] McDougall, N. M., Cumpsty, N. A., Hynes, T. P., 1990. "Stall Inception in Axial Compressors". *Journal of Turbomachinery*, **112**, pp. 116-123

[11] Garnier, V. H., Epstein, A. H., Greitzer, E. M., 1991, "Rotating Waves as a Stall Inception Indication in Axial Compressors", *Journal of Turbomachinery*, **113**, pp. 190-301

[12] Fink, D. A., Cumpsty, N. A., Greitzer, E.M., 1992. "Surge Dynamics in a Free-Spool Centrifugal Compressor System". American Society of Mechanical Engineers

[13] di Mare, L., Krishnababu, S. K., Mück, B., Imregun, M., 2009. "Aerodynamics and aeroelasticity of a HP compressor during surge and reversed flow", Proceedings of the 12th International Symposium on Unsteady Aerodynamics, ISUAAAT12, S9.4

